Characterization of argon dielectric barrier discharges applied to ethyl lactate plasma polymerization

Morgane Laurent[1,2,3], Edouard Desjardins[4], Maximilian Meichelboeck[1,2], Nicolas Naudé[3], Luc Stafford[4], Nicolas Gherardi[3], and Gaétan Laroche[1,2]

[1]Laboratoire d'Ingénierie de Surface, Centre de Recherche sur les Matériaux Avancés, Département de génie des mines, de la métallurgie et des matériaux, Université Laval, 1045, avenue de la Médecine, Québec G1V 0A6, Québec, Canada
[2] Centre de recherche du CHU de Québec, Hôpital St François d'Assise, 10, rue de L'Espinay, Québec G1L 3L5, Québec, Canada
[3] LAPLACE, Université de Toulouse, CNRS, INPT, UPS, France
[4] Département de Physique, Université de Montréal, Montréal, Québec H3C 3J7, Canada

ABSTRACT
The influence of the input voltage frequency (35 and 150 kHz), interelectrode gap (1 and 2 mm) and precursor concentration (250, 350, and 450 ppm) on the electron temperature (T_e), number density of metastable Ar atoms ($n(Ar^m)$), and discharge current density (proportional to the electron density ne) is studied in an argon-ethyl lactate dielectric barrier discharge (DBD). An argon-ammonia Penning mixture is also considered as reference. These results are correlated to the chemistry (XPS, IR) and topography (AFM) of the ethyl-lactate-based plasma polymer coatings. Low T_e values from 0.3 to 0.5 eV were obtained for all discharges. This observation, in addition to resemblances with the Ar-NH_3 mixture, suggested that the ionization kinetics of ethyl lactate-based discharges is driven by Penning reactions. Among the investigated parameters, the dissipated power obtained through changes of the excitation frequency had the largest impact on both the coatings properties and the discharge behavior.

KEYWORDS
dielectric barrier discharge (DBD), electron temperature, electron density, argon metastable, ethyl lactate, optical emission spectroscopy

CITATION
Laurent, M., Desjardins, E., Meichelboeck, M., Naudé, N., Stafford, L., Gherardi, N., & Laroche, G. (2017). Characterization of argon dielectric barrier discharges applied to ethyl lactate plasma polymerization. Journal of Physics D: Applied Physics, 50(47), 475205.

1 INTRODUCTION

Electron number density and temperature (T_e), number density of excited and reactive species are often used to characterize plasmas because they are accurate ways to quantify the energy available in a non-local thermal equilibrium plasma and hence deduce possible chemical reaction pathways [1]. In particular, the measurement of these parameters can be a powerful approach to reproduce plasma conditions for materials processing (for example, the deposition and functionalization of thin films) even with different experimental setups. This could be very useful, in particular during reactor upscaling for industrial applications. However, if the electron temperature

can rather easily be obtained in low-pressure plasmas using a Langmuir probe, the extraction of T_e values in higher-pressure plasmas is much more complex since the non-collisional plasma sheath theories required for detailed analysis of current-voltage characteristics do not hold at such pressures [2–6]. To circumvent this limitation, high-pressure plasmas are generally characterized by optical diagnostics, including optical emission spectroscopy, optical absorption spectroscopy, and laser-induced fluorescence.

Optical emission spectroscopy (OES) is widely used because it enables to obtain the emission spectra of atoms and molecules with a relatively inexpensive and non-invasive set up. Measurement of OES line emission intensities, when combined with a collisional-radiative model describing the populations of excited states, enables to extract the variation of T_e throughout the evolution of the discharge [7–11]. This approach consists in building a population model for various excited levels accounting for all population and depopulation processes. By resolving the corresponding set of particle balance equations for at least two different energy levels, it is possible to extract the number density ratio of both levels. In some cases, this ratio becomes solely dependent on the electron temperature, such that T_e can be obtained from a simple line ratio measurement. In other cases, line ratios are also linked to the population of other excited species such that more than one-line ratio is required to obtain T_e and the population of the corresponding excited species. This is the case when stepwise excitation processes involving metastable species play an important role in the population kinetics. To accurately determine all of these parameters from OES spectra, the best solution is to rely on a very large number of lines emanating from various excited states. This method has been widely used over the last thirty years for both low- and atmospheric-pressure plasmas. In many cases, excellent agreement was observed between the values of T_e obtained from OES with respect to those obtained from other techniques such as Langmuir probes or discharge electrical models [10].

In most studies reported in literature, OES analysis used to extract T_e values in non-equilibrium plasmas at atmospheric pressure are realized in rare gases such as He or Ar and over a very narrow range of operating conditions. In addition, no studies were realized in presence of reactive precursors used for plasma-enhanced chemical vapor deposition of functional coatings. Therefore, it is currently impossible to establish convincing correlations between these fundamental properties describing the electron kinetics and either the discharge regime or the physico-chemical properties of plasma-deposited coatings.

The influence of the excitation frequency on the discharge regime of argon-ammonia mixtures has already been examined by different studies: higher frequency yields Townsend-like discharges while lower frequency leads to glow dielectric barrier discharges [12]. The frequency of the applied voltage, known to promote the easy dissipation of power, revealed effects on the growth rate and on the chemical composition of plasma-deposited organic or organosilicon thin films [13–15]. The gap between the electrodes was also demonstrated to have an influence on the discharge regime, especially due to gas flow and capacitance modifications [16]. For instance, in helium discharges, a Townsend discharge mode usually occurs at smaller gap while larger gaps tend to facilitate the glow discharge regime [17]. Moreover, Motret et al. demonstrated that the gas mixture influenced the OH(A) rotational temperature in Ar-H_2O dielectric barrier discharges, especially at very high concentrations (>10000 ppm of water) [18]. From a coating point of view, Massines et al. found no change in the chemical composition of plasma-deposited thin films when varying the oxidant-to-organosilicon ratio above a certain critical value in a nitrogen discharge, but established a linear correlation with the growth rate, as also observed by Enache et al. [14,19].

In this study, the influence of the plasma frequency (f), interelectrode gas gap (g), and precursor concentration was examined in argon-ethyl lactate dielectric barrier discharges. When introduced into an electrical discharge, this ethyl lactate precursor has already shown a strong potential to synthesize poly(lactic acid)-like coatings relevant for biomedical applications [13,20,21]. More precisely, the first part of this work aimed at evaluating the influence of the aforementioned parameters on the electron temperature (T_e), number density of argon metastable atoms ($n(Ar^m)$),

and the current density (J). The argon collisional-radiative model used in this work to analyze 4p-to-4s Ar transitions was adapted from the model developed for helium n = 3 levels by Gangwar et al. [11] It assumed a Maxwellian electron energy distribution function and considered: (1) electron-impact processes from both ground and excited argon states; (2) excitation transfers between 4p states upon collisions with ground state argon atoms; (3) spontaneous emission from argon 4p states; (4) collision quenching of argon 4p states by argon ground state atoms and impurities; 5-radiation trapping of argon 4p-to-4s transitions [22]. For comparison purposes, an argon-ammonia (Ar-NH_3) discharge, which is known to form a Penning mixture, was also studied in the same electrical conditions as the argon-(ethyl lactate) (Ar-EL) discharge [23]. The second part of the investigation intended to correlate the discharge properties, obtained from the combination of OES, collisional-radiative model, and detailed analysis of the current-voltage characteristics, with the physico-chemical properties of the plasma-deposited coatings. The layers were topographically characterized by atomic force microscopy, while their chemistry was assessed using Fourier Transform Infrared and X-ray Photoelectron spectroscopies.

2 METHODS

2.1 Atmospheric pressure plasma conditions

2.1.1 Plasma reactor and electric diagnostics

A plane-to-plane dielectric barrier discharge reactor was used with two 0.64 mm-thick alumina plates as dielectrics, a 1.1-mm thick glass plate as substrate, and a gas gap varied between 1.1 and 2.1 mm. To facilitate the reading, those gas gaps will later on be referred to as 1 and 2 mm respectively. Before each experiment, the reactor was put under vacuum and then filled with argon (Ar, 99.999 %, Alphagaz 1, Air Liquide) to reach atmospheric pressure. Argon was then injected between the dielectrics at a flow rate of 2 $L.min^{-1}$.

The voltage applied to the 3.9 × 3 cm^2 electrodes was measured using a high-voltage probe (Tektronix P6015A) and a 220 nF capacitor in series with the cell discharge was used to monitor the electric charge. These signals were visualized on a digital oscilloscope (Teledyne Lecroy, WaveRunner 8404M-MS, bandwidth: 4 GHz, 40 GS/s). The dissipated discharge power P_w per surface unit ($W.cm^{-2}$) was calculated using Q-V Lissajous plots [24]. The current density (J) were calculated from the mean current value during the discharge current peak divided by the surface of the discharge (3.9 × 3 cm^2).

2.1.2 Power supplies

For low-frequency measurements, a 35 kHz sinusoidal voltage was generated (Agilent, 33210A) and amplified with a linear amplifier (Crest Audio model 4801) whose output is applied to the primary of a transformer (Boige et Vignal, ratio 1:30).

The DBD could also be powered by a high frequency (150 kHz) power supply (RFPP-LF 10) associated with a homemade matching network. The voltage is amplified using a transformer (ratio 1:20). The power supply is controlled in power and not in voltage. The electrodes are connected to the secondary of the transformer.

Correlation between coating properties and plasma experimental parameters was performed by calculating the energy E transmitted to the molecules (corresponding to the energy per volume unit) using equation 1, with P_w, g and tr being the dissipated power, the interelectrode gap, and the mean residence time of a molecule in the plasma, respectively [13].

$$E(J \cdot cm^{-3}) = \frac{P_w(W \cdot cm^{-2})}{g(cm)} \cdot t_r(s) \quad (1)$$

2.1.3 Gas mixtures

An (-)-ethyl L-lactate precursor (98 %, Sigma Aldrich) was injected through a nebulizer (Mira Mist CE, Burgener Reserch Inc.) using a syringe pump (Legato 110, Fisher Scientific) to reach 250, 350 or 450 ppm in the argon flow, and deposited on the substrates. For the optical emission spectroscopy measurements described below, the argon-ethyl lactate discharge was compared to an argon-ammonia discharge, which is known to be a Penning mixture, when using the low frequency power supply. 40 sccm of Ar + (0.998 ± 0.05) % NH_3 (Air Liquide) were thus added to the nominally pure argon flow to obtain a final concentration of 200 ppm of ammonia in the gaseous environment.

2.1.4 Conditions tested

The various conditions tested are summarized in Table 1. The condition using ethyl lactate, 250 ppm, 1 mm gap, and a frequency of 35 kHz was used as reference. All other conditions were derived from there by varying one parameter at a time.

Table 1. Plasma deposition conditions tested

Molecule X mixed with argon	**[X]** ppm	**g** mm	**f / P_w** kHz/W.cm^{-2}
Ammonia	200	1	35 / 0.15
Ethyl lactate	250	1	35 / 0.15
Ethyl lactate	250	1	150 / 0.8
Ethyl lactate	250	2	35 / 0.15
Ethyl lactate	350	1	35 / 0.15
Ethyl lactate	450	1	35 / 0.15

2.2 X-ray Photoelectron Spectroscopy (XPS)

A PHI 5600-ci spectrometer (Physical Electronics) was used to perform the coating surface analysis. For surface survey measurements, the XPS source used was a standard aluminum anode (1486.6 eV) operated at 200 W with a charge neutralizer to record spectra between 0 and 1200 eV. Samples were divided in three identical areas of about 1 x 1 cm^2 along the gas flow, to follow the surface chemistry of the coatings throughout many plasma regions. Three measurements were performed on each of these 1 cm^2 areas to ensure reproducibility.

2.3 Attenuated Total Reflectance Fourier Transformed Infrared spectroscopy (ATR-FTIR)

Spectra were recorded with a FTIR spectrophotometer (Cary 660, Agilent Technologies) equipped with a deuterated L-alanine-doped triglycine sulfate (DLaTGS) detector and a potassium bromide (KBr) beam splitter. Each spectrum was the result of 128 interferograms that were co-added, apodized with a Blackmann-Harris 4 term function, and Fourier transformed to yield a 4 cm^{-1} spectral resolution. A SplitPeaTM ATR microsampler (UNS-ATR-0E, Harrick Scientific Products) equipped with a Si crystal was used to record the spectra from 4000 to 400 cm^{-1}. For each layer, three equally distributed points were measured along the center of the coating in the flow direction at 0.5, 1.5 and 2.5 cm from the entrance of the carrier gas in the plasma zone.

2.4 Atomic Force Microscopy (AFM)

A Dimension 3100 Atomic Force Microscope from Digital Instruments was used in tapping mode supplied with a NCHV probe from Bruker. Surface topography of 10 x 10 μm^2 representative AFM images were analyzed using NanoScope Analysis v.1.40 software from Bruker. The average roughness (R_a) and root mean square roughness (R_q) were recorded for all surfaces.

2.5 Optical Emission Spectroscopy (OES)

The optical system comprised a spectrophotograph from Princeton Instruments (Acton) coupled to a PI-Max3 intensified charged coupled device camera also from Princeton Instruments. An optical fiber enabled to bring the optical system close to the plasma, perpendicularly to the 1 mm-thick quartz block guiding the gas flow at about 1 cm from the gas entrance in the plasma zone (and 2 cm from its exit). A BLZ 300 monochromator was used to gather spectra from 650 to 950 nm with a 10 nm overlap region. Each time-resolved spectrum was recorded successively with 100 ns gate, so that the whole period of time around the discharge peak was covered. Each spectrum represents the sum of 1000 spectra at 35 kHz and 200 spectra at 150 kHz taken at the same time referentially to the current-voltage characteristics. For each spectrum, the wavelength axis was centered according to the 763 nm peak and the overall spectral intensity was corrected to take into account the optical response of the optical fiber, spectrograph, and camera.

2.6 Collisional-radiative (CR) model

For all investigated conditions, the most probable pair of electron temperature (Te) and number density of argon metastable atoms ($n(Ar^m)$) were obtained from the measured optical emission spectra using a recently-developed argon collisional radiative model [22]. This model solves the particle balance equation for the 10 argon 4p levels. It takes into account population processes by electron impact with a ground state argon atom to populate a 4p level, electron impact with an excited 4s state to populate a 4p level, as well as 4p-neutral collisions to populate another 4p level (excitation transfer processes). The model also considers the following depopulation processes of argon 4p states: spontaneous emission, collisional quenching by ground state argon atoms and impurities, and radiation trapping of argon 4p-to-4s transitions. For these calculations, T_e and $n(Ar^m)$ are the only adjustable parameters. It is worth mentioning that argon 4s states were treated as a block, which means that their population was assumed equal for all experimental conditions.

The measured emission intensities were then fitted with this model using T_e and $n(Ar^m)$ as the only adjustable fitting parameters. This was realized by computing emission intensities over a wide range of T_e and $n(Ar^m)$ values and by calculating a percentage standard error between measured and calculated emission intensities. The values of T_e and $n(Ar^m)$ that minimized the percentage standard error were then attributed to the corresponding set of experimental conditions. In this work, 12 argon 4p-to-4s transitions were considered. These lines were chosen based on availability of cross sections for the population and depopulation processes of these excited states and the spectral resolution of our monochromator during the experiments. More precisely, if the lines were distinguishable from the background noise by at least 50% of the calculated background, they were then considered in the fitting operation. Values of T_e and $n(Ar^m)$ extracted from the optical emission spectra in operating conditions for which less than 12 lines were available, either due to low emission signals or highly convoluted lines, were not used in this study.

3 RESULTS

3.1 Plasma composition

The argon discharges analyzed by optical emission spectroscopy demonstrated the same argon characteristic peaks in $Ar+NH_3$ and in Ar + EL mixtures. The corresponding emission lines are

detailed on the Ar energy diagram presented in Figure 1. All lines originated from transitions from the $3p^5 4p$ excited levels (levels $2p_1$ to $2p_{10}$ in Paschen notation), characterized by energies in the range of 12.91 to 13.48 eV, to the metastable ($1s_3$ and $1s_5$) and resonant ($1s_2$ and $1s_4$) $3p^5 4s$ levels with energies between 11.55 and 11.83 eV [25].

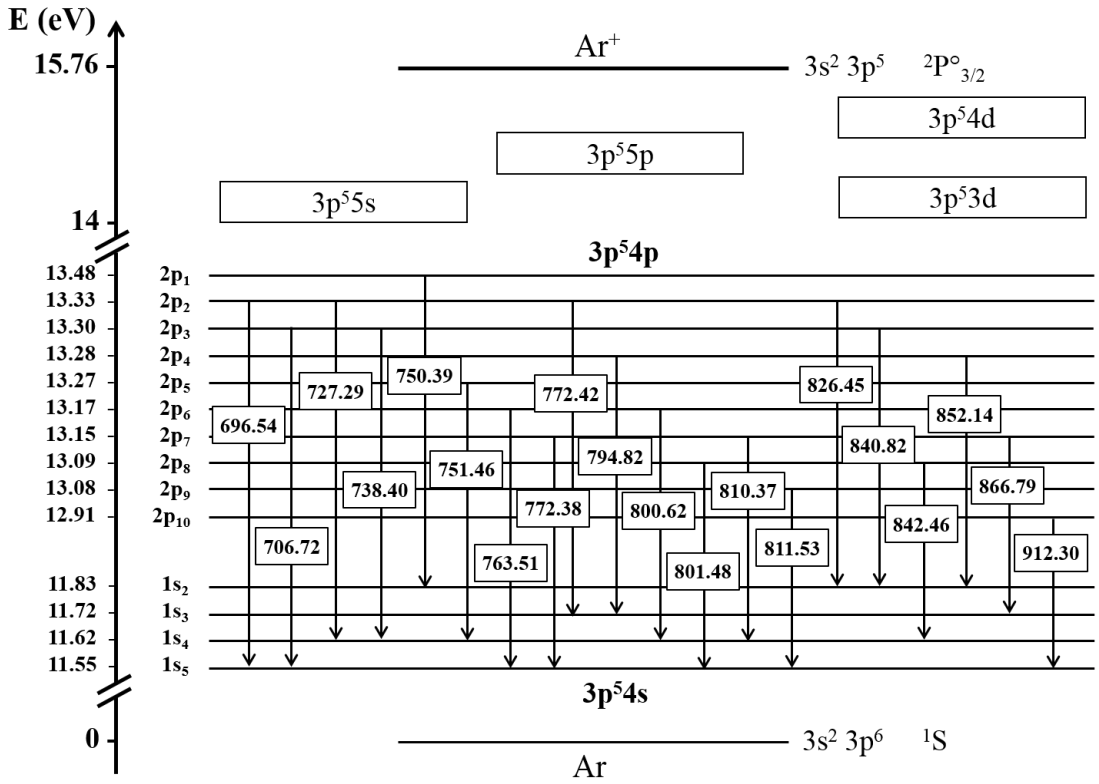

Figure 1. Argon energy diagram along with the 4p-to-4s transitions observed by optical emission spectroscopy. All wavelengths are in nm.

The voltage-current curve obtained at 35 kHz with a 250-ppm ethyl lactate-argon discharge is shown in Figure 2a along with the spectrometer synchronized gate in blue. The time position of the gate shown in this figure at t = 30 µs corresponds to the delay used to capture the first OES spectrum during a gate of 0.1 µs in Figure 2b. In this figure, the set of time-resolved optical emission spectra was taken around the discharge current peak. The intensity of each peak increased with time up to a maximum before decreasing once the discharge current peak elapsed. As expected, this confirmed the presence of excited $3p^5 4p$ species in higher concentrations in the maximum current density range. However, this maximum intensity detected by emission could be reached at slightly different times depending on the transition line observed. Moreover, line ratios were clearly varying depending on the period studied. For instance, the 763 nm line, characteristic of the $2p_6$-to-$1s_5$ transition, first appeared as the most intense transition line observed at the beginning of the discharge but was then overtook by the 772 nm line, which was made of two transitions coming out at 772.38 ($2p_7$-to-$1s_5$) and 772.42 ($2p_2$-to-$1s_3$) nm. These peak intensity variations were identically observed for both current peak directions (positive and negative) and seemed rather symmetrical around the discharge peak time for all conditions examined in this study. These qualitative observations were analyzed in more details using the CR model.

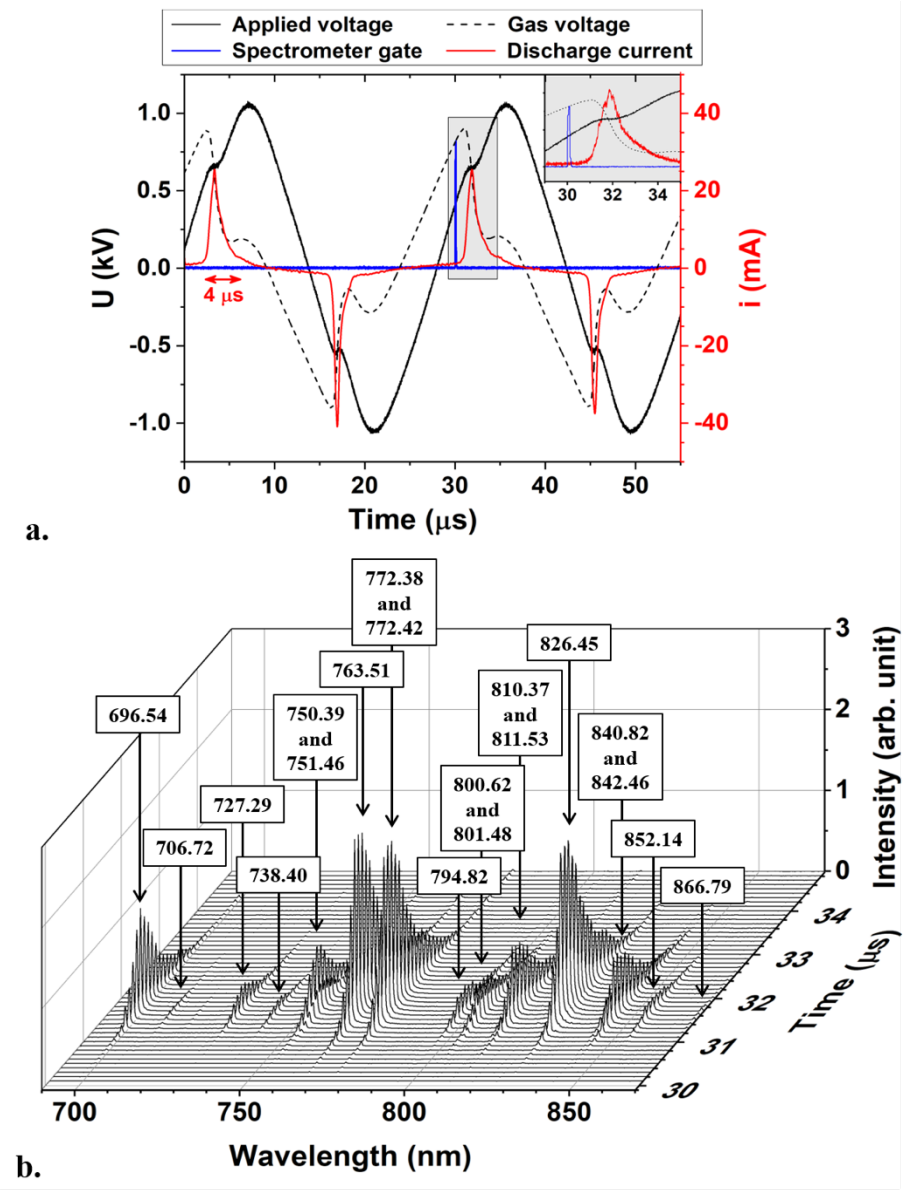

Figure 2. a. Voltage-current curve of an argon (250 ppm)/ethyl lactate discharge generated using a 35 kHz signal, with 1 mm gap; b. Time resolved spectra of the corresponding discharge analyzed by OES with the peak attributions.

3.2 Correlation of electron temperature, current density, and Ar metastable density in the plasma with the XPS O/C ratio in the coatings

For all conditions examined in this study, the most probable pair of T_e and $n(Ar^m)$ were obtained by fitting the measured optical emission intensities with the CR model [22]. Time-resolved values were then averaged for both discharge peaks (positive and negative half cycles), and the mean between those two time-averaged values was plotted. As shown below, the mean T_e and $n(Ar^m)$ values were in the range of 0.3-0.5 eV and ~10^{11}-10^{12} cm^{-3}, respectively. The influence of the frequency of the applied signal, the precursor concentration, and the gap between the electrodes on T_e (in eV), J (in $mA.cm^{-2}$), and $n(Ar^m)$ (in cm^{-3}) are presented in Figures 3, 4, and 5.

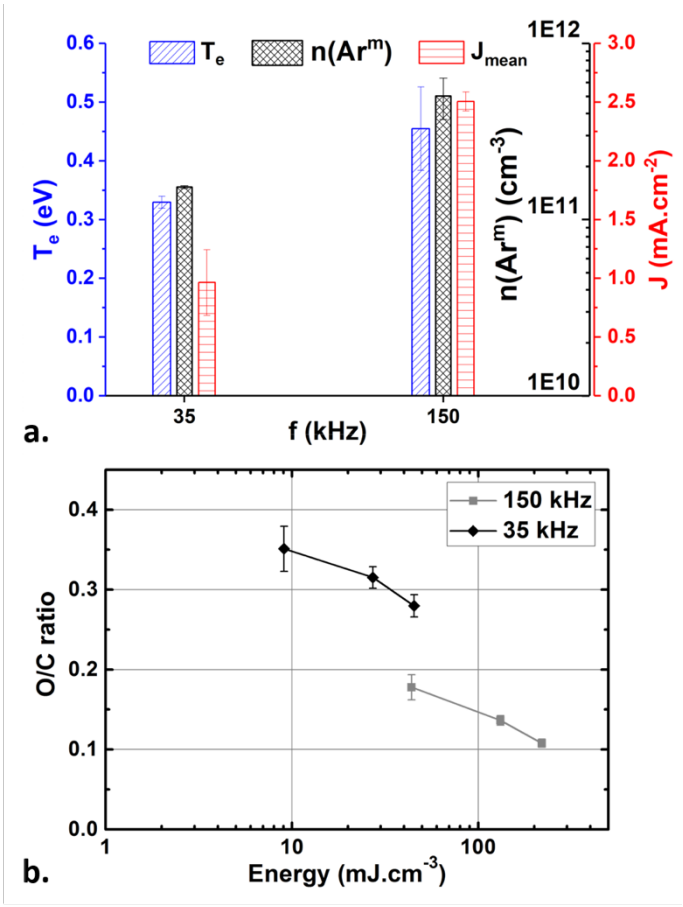

Figure 3. Influence of the frequency/power input in an Ar-EL plasma (1 mm gap, 250 ppm) and coating chemistry. a. Evolution of the electron temperature, the number density of Ar metastable atoms (both extracted from the comparison between measured and simulated emission intensities) and the mean current density (averaged during the discharge current peak); b. Evolution of the oxygen/carbon ratio at the corresponding coating surface (obtained from XPS) as a function of the energy submitted to the molecules.

Figure 3a presents the influence of the input voltage frequency on the electron temperature, the number density of metastable argon atoms, and the current density. It can be seen that by increasing the voltage frequency from 35 kHz (P_w = 0.15 W.cm^{-2}) to 150 kHz (P_w = 0.8 W.cm^{-2}) led to a rise in the mean electron temperature (from 0.33 to 0.45 eV) and the mean number density of metastable argon atoms (from 1.5 to $5 \cdot 10^{11}$ cm^{-3}). The mean discharge current density, which is directly proportional to the electron density , also increased with the frequency.

Figure 3b displays the XPS O/C ratio of the corresponding coatings as a function of the volume energy injected into the discharge obtained from Equation (1). The three energy points for each coating represent different positions along the gas flow lines, the lowest energy being located at the entrance of the plasma zone and the highest at the exit of the plasma zone. It is obvious that the more energy was applied to the precursor molecules, the more carbonated the layer ended up. Moreover, as expected, working at higher frequency, which also implies applying a higher energy, led to the synthesis of more carbonated coating as going from 35 kHz to 150 kHz shifted the O/C ratio curve down by about 0.17.

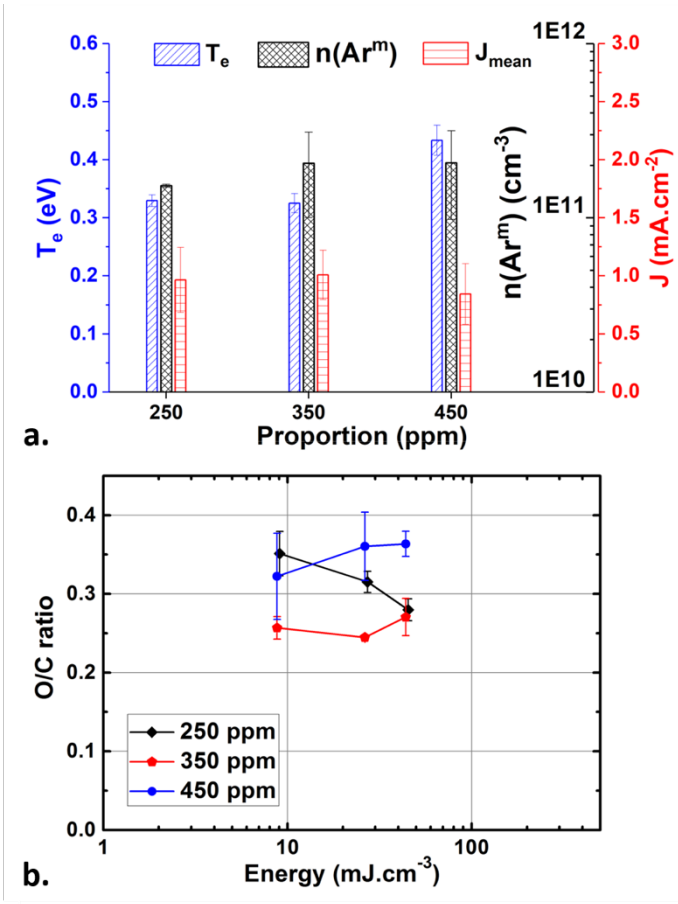

Figure 4. Influence of the precursor proportions on the plasma (1 mm gap, 35 kHz, 2 kV, 0.15 $W.cm^{-2}$) and coating chemistry. a. Evolution of the electron temperature, the number density of Ar metastable atoms (both extracted from the comparison between measured and simulated emission intensities) and the mean current density (averaged during the discharge current peak); b. Evolution of the oxygen/carbon ratio at the corresponding coating surface (obtained from XPS) as a function of the energy submitted to the molecules.

Figure 4a exhibits no significant difference in electron temperature when increasing the precursor amount from 250 to 350 ppm. However, a further rise of the precursor concentration from 350 to 450 ppm led to a slight but significant increase of T_e by 0.1 eV. Given the large standard deviation between the positive and negative half cycles, the variation of $n(Ar^m)$ and ne observed when increasing the amount of precursor was not considered as significant.

Figure 4b shows no obvious trend when increasing the precursor concentration. The 350-ppm coating appeared to be more carbonated than the 250-ppm one, except for the exit zone (at higher energies). The 450-ppm layer seemed to be rather heterogeneous even among the same 1 cm^2 area, particularly at the entrance of the carrying gas. The exit zone of this layer contained more oxygen than the other coatings at the same energy.

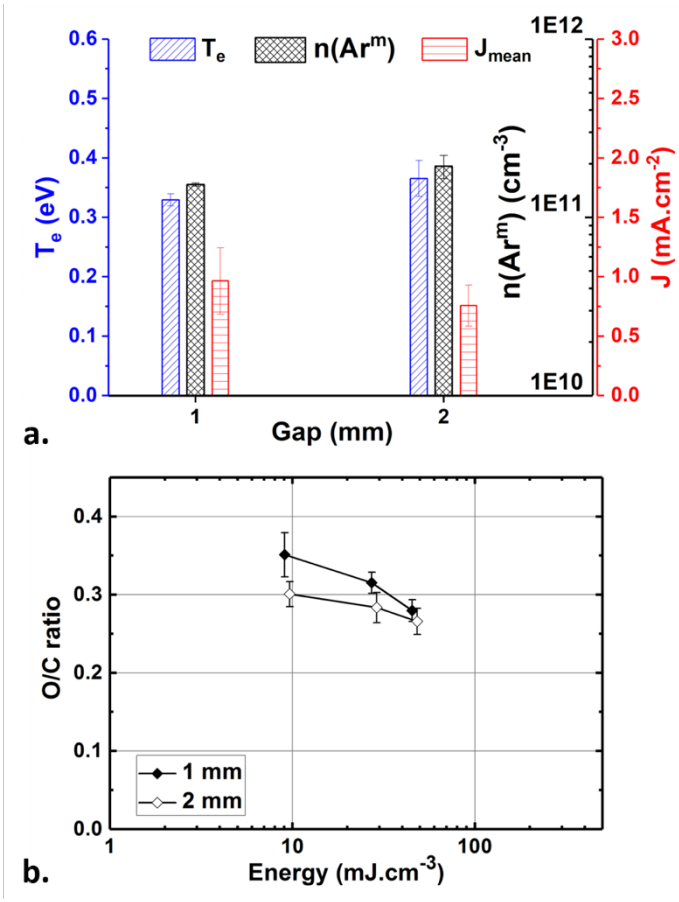

Figure 5. Influence of the interelectrode gas gap in the Ar-EL plasma (35 kHz, 2 kV) and coating chemistry. a. Evolution of the electron temperature, the number density of Ar metastable atoms (both extracted from the comparison between measured and simulated emission intensities) and the mean current density (averaged during the discharge current peak); b. Evolution of the oxygen/carbon ratio at the corresponding coating surface (obtained from XPS) as a function of the energy submitted to the molecules.

Figure 5a exhibits no major variation in T_e, $n(Ar^m)$, and J when increasing the gap between the electrodes from 1 to 2 mm. Similarly, the O/C ratio of the coatings, displayed by Figure 5b, were not significantly affected by the gap increase, apart from the lowest energy analysis point which had a slightly higher carbon content compared to their homologous using the same conditions at 1 mm as shown by Figure 5b. Of note, with a 2 kV voltage applied, the corresponding electrical power were 0.15 $W.cm^{-2}$ when using a 1 mm gas gap and 0.19 $W.cm^{-2}$ with a 2 mm gap.

Figure 6a presents a comparison of the argon-ethyl lactate discharge studied with an argon Penning mixture made of 200 ppm of ammonia in the same electrical and gap conditions. The results obtained from OES measurements combined with the model showed no difference for both T_e and $n(Ar^m)$ when using NH_3 instead of ethyl lactate. However, the current density was found to be much lower in the case of the argon and ammonia mixture compared to the ethyl lactate-argon discharge. This translates the presence of multiple discharge peaks in the current, leading to a much longer discharge on-time and hence to a lower mean current value.

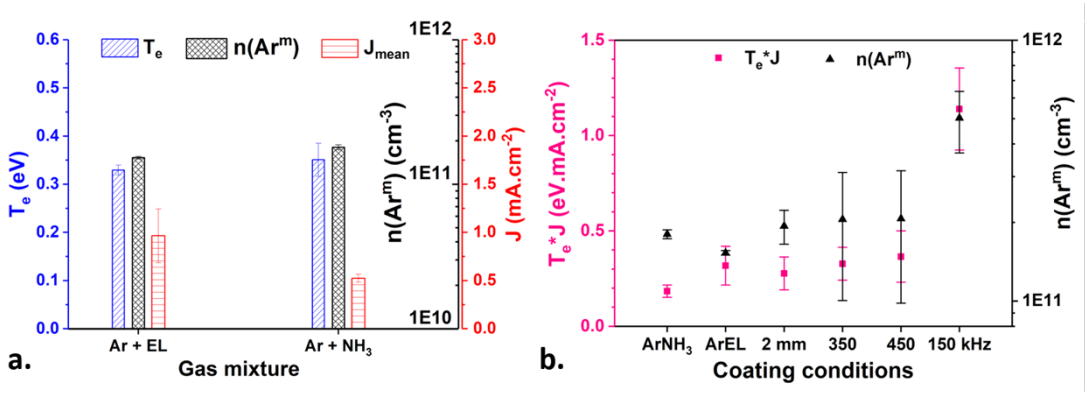

Figure 6. a. Comparison of the argon-ethyl lactate discharge (250 ppm, 1 mm, 35 kHz, 2 kV 0.15 W.cm^{-2}) and an argon-ammonia discharge (200 ppm, 1 mm, 35 kHz, 2 kV, 0.15 W.cm^{-2}); b. Evolution of the electron behavior (translated by electron temperature * current density) along with the argon metastable levels population with all conditions.

Figure 6b gathers all conditions studied to compare the influence of the electrons versus argon metastable species during plasma polymerization of ethyl lactate in argon-based dielectric barrier discharges. Two obvious groups appear among the ethyl lactate argon discharges: the first one at "low energy" in terms of both electrons and metastable behaviors with the discharges happening at 35 kHz. The second one at "higher energy" contains only the discharge studied at 150 kHz. The Ar-NH_3 discharge presents similar characteristics with the argon-ethyl lactate mixture in the same energetic conditions.

3.3 Coating properties

3.3.1 Roughness analysis

As presented in Figure 7, the AFM analysis of the ethyl lactate coatings obtained in argon-based dielectric barrier discharges demonstrated a difference in roughness depending on the working frequency. It is obvious that increasing the frequency up to 150 kHz (corresponding to P_w = 0.8 W.cm^{-2}), led to a huge powder formation. This translates into an increase of the average roughness (R_a), which went from 0.3 nm for all positions of the coating made at 35 kHz, and a gap of 1 mm to values ranging between 0.7 and 5.4 nm for the layer made at 150 kHz.

When increasing the gap at 2 mm, the formation of small particles of a few hundred-nanometers in diameter was noticed at the entrance of the plasma zone, which led to a small increase of the Ra up to 0.8 nm. The rest of the coating provided similar Ra values to its homologous made using a 1 mm gap.

It is worth mentioning that the coating deposited using 450 ppm of ethyl lactate appeared oily and so smooth that any contact with the coating could leave a mark. The same texture was observed towards the exit of the 350-ppm coating (zone corresponding to the red pentagon at the highest energy in Figure 4b).

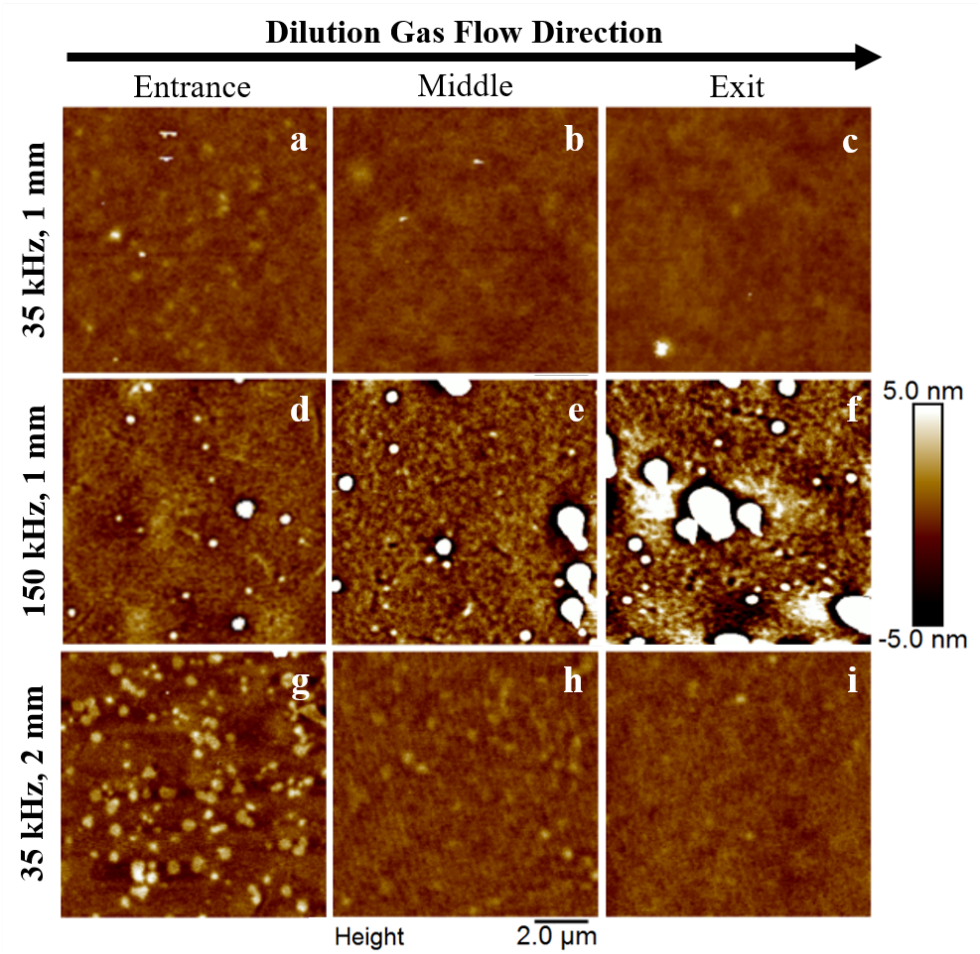

Figure 7. AFM analyses of the argon-ethyl lactate coating synthesized at 35 kHz and 0.15 W.cm^{-2}, using 1 mm (a, b, and c) and 2 mm (g, h, and i) gaps and the coating synthesized at 150 kHz, 0.8 W.cm-2, with a 1 mm (d, e, and f) gap, depending on the position along the gas flow

3.3.2 Chemical composition

The IR spectra of the layers made at 250 ppm, presented in Figure 8, displayed peaks at 1730 cm^{-1}, which were assigned to the carbonyl (C=O) stretching mode of ester (COOC) groups. The corresponding C-O stretching vibration from these same groups was observed at 1270 cm^{-1}. Features from 2785 to 3025 cm^{-1} and from 1315 to 1510 cm^{-1} were assigned to various C-H stretching and bending modes in methyl and methylene groups, respectively. From a more detailed peak analysis, the presence of -CH_3 (with its asymmetric/symmetric stretching modes at 2955/2875 cm^{-1} and both asymmetric/symmetric bending modes at 1460/1375 cm^{-1}), >CH_2 (from peaks at 2935 cm^{-1} -asymmetric stretch-, at 2855 cm^{-1} -symmetric stretch and 1460 cm^{-1} -bending mode), and >CH- (from overlapped peaks at 2895 cm^{-1} -stretch- and 1350 cm^{-1} -bend-) was demonstrated [26]. In addition, the stretch of an H bonded hydroxy group was observed via the broad band from 3150 to 3670 cm^{-1}.

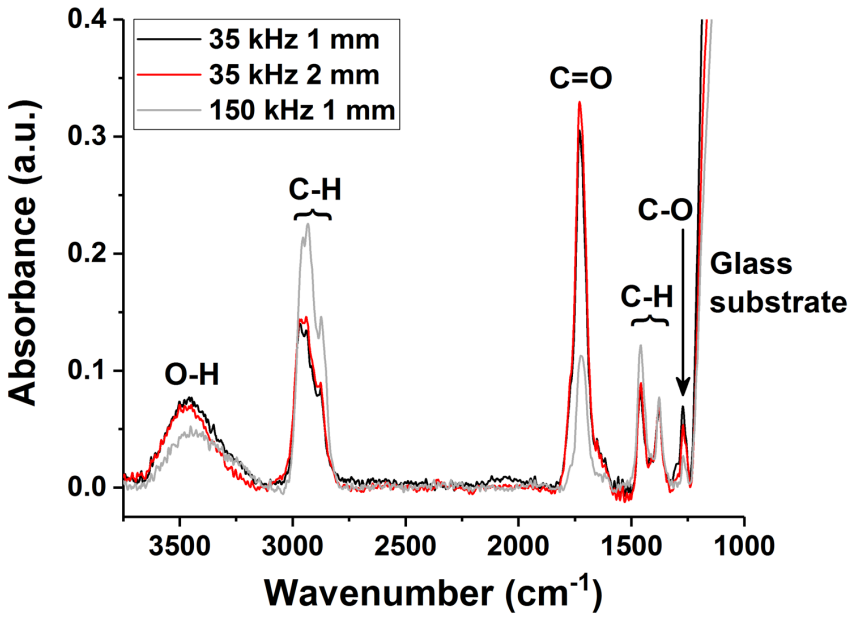

Figure 8. Comparison of the infrared spectra coatings made at 35 kHz with 1- and 2-mm gap and at 150 kHz with 1-mm gap.

In order to compare the three conditions studied in a quantitative way, the spectra were normalized to the thickness of the corresponding coating at the position of the analysis. No difference was observed between the 250 ppm coatings obtained with gaps of either 1 or 2 mm. However, a clear variation was observed when changing the frequency from 35 to 150 kHz. Indeed, a clear absorbance increase of the C-H stretching bands was observed while the C=O stretching mode absorbance was subjected to a significant decline concomitant with the intensity of the C-O and O-H stretching mode features. In fact, the ratio of the peaks C=O/C-H (stretch) were found to be below 1 for all coatings obtained at 35 kHz but above 1 for 150 kHz. The coating made at 450 ppm presented similar properties with its homologous made at 250 ppm, but with much lower signals.

4 DISCUSSION

The excited species observed in argon-ethyl lactate and argon-ammonia discharges through optical emission spectroscopy between 650 and 950 nm were mostly attributed to argon excited species based on NIST referenced emission lines [27].

Mean values of electron temperatures (around 0.3-0.5 eV) and number densities of argon metastable species (between 10^{11} and 10^{12} per cm^3) obtained from the comparison between measured and simulated line emission intensities are comparable to what was recently reported for helium discharges operated under similar conditions [11]. T_e values are also very close to those obtained in argon microwave discharges at atmospheric pressure (0.5-0.7 eV) but lower than those obtained in the jet of an Ar-NH_3 plasma (0.9 eV) [5,28]. This latter difference with the jet configuration can most likely be attributed to the presence of N_2 and O_2 due to open-air configuration; this aspect was already discussed by Levasseur et al. in He-based discharges.[29] The same Ar-NH_3 jet study also reported Ar metastable number densities in the range of 10^{11} and 10^{12} cm^{-3}, which is in agreement with the values obtained in this work and those expected for glow dielectric barrier discharges (10^{11} cm^{-3}).[14,28] Another study reported argon atom metastable densities of 4.10^{13} cm^{-3} in an Ar-NH_3 discharge powered with 1.2 $W.cm^{-3}$ at 15 kHz, which is 100 times higher than the values obtained in this study using similar dissipated volume powers (1.5 $W.cm^{-3}$ with the 35 kHz, 1

mm) [30].This increase likely comes from a difference in the discharge regime since the large current peak duration (25 µs) reported by this group indicates the behavior of a Townsend discharge, which is known to be characterized by much higher metastable number densities [14].

Ionization by electron impact collisions with ground state argon atoms requires electron energies above 15.76 eV, which is much higher than the electron temperature values obtained for all the discharges examined in this study. However, it is worth mentioning that the T_e values presented in this paper represent an average value of the electron energy. Even at low electron temperatures, there is, in principle, a population of high-energy electrons in the electron energy distribution function that could contribute to the ionization of argon atoms directly from ground state. However, for the low mean electron temperatures obtained in this study, assuming a Maxwellian distribution, most electrons do not have a sufficient energy to induce direct ionization from ground state. The large Ar metastable number densities combined with the relatively high proportion of ethyl lactate inside the gas phase indicates that ionization phenomena would more likely proceed through a Penning mechanism. This would result in the formation of the ethyl lactate positive ion, which was reported to have an energy level at 10.3 eV [31]. Consequently, this ion would likely be the most abundant in the Ar-(ethyl lactate) plasmas. This hypothesis is further supported by the strong diminution of the breakdown voltage observed, since the applied voltage necessary to initiate a discharge with this system went from 3.2 kV_{pp} in a pure argon discharge with a 1 mm gap down to 1.7 kV_{pp} in presence of ethyl lactate.

When applied to the Ar-ammonia discharge (which is known to be a Penning mixture), the comparison between measured and simulated line emission intensities provided comparable results for Ar-(ethyl lactate) and Ar-ammonia discharges in terms of electron temperatures and number densities of metastable argon atoms. In the experimental conditions examined in this work, the main reaction products are expected to be $NH^{\bullet}$ and $NH_2^{\bullet}$ radicals as well as NH_3^+ ions by Penning ionization.[30] The current density variation observed between Ar (ethyl lactate) and Ar-ammonia discharges were mainly due to changes in the shape of the discharge current with the appearance of a second broad peak in the presence of ammonia. This suggests that the argon-ammonia discharge is a better Penning mixture than argon-ethyl lactate, which translated into a lower breakdown voltage (1.0 kV_{pp}) and hence a longer discharge. This was previously observed by other groups and attributed to an additional electron impact excitation route involving NH3 when using low concentration of ammonia.[30]

The results presented in Fig. 3 showed that a higher frequency led to higher electron temperatures and densities, and argon metastable densities. A higher frequency, generally implying a higher power input in the plasma, has previously been correlated to a higher energy submitted to the precursor molecules [13]. OES results suggest that the greater energy available at 150 kHz (optical measurement made at an energy equivalent to 94 $mJ.cm^{-3}$ for 150 kHz compared to 18 $mJ.cm^{-3}$ for 35 kHz) is transported through both electrons - thanks to their larger number density (larger J implying larger n_e) combined with their increased average energy (linked to T_e) - and metastable species ($n(Ar^m)$). Looking at the ratio of the $n(Ar^m)$ value at 150 kHz to its value at 35 kHz, one obtains 3.4. On the other hand, J and T_e only increase by a factor of 1.2 and 1.4 between 35 and 150 kHz. This indicates that the metastable contribution increased much more than the one of the electrons, which could be explained by a more pronounced memory effect happening at higher frequencies [16]. It also indicates that metastable species still have quite an influence in the discharge regime at 150 kHz and likely play a significant role in the plasma deposition process through stepwise ionization processes [16]. This can be correlated with the coating itself. As expected, using a higher frequency, which is also equivalent to applying a higher energy (for the same position of analysis), resulted in a higher roughness as well as a more carbonated coating with less ester functionalities, as shown by both XPS and IR analyses. This is in correlation with what was previously observed when increasing the energy submitted to the molecules [13]. Moreover, even at similar energies, when comparing the highest energy point obtained at 35 kHz (at the exit of the carrier gas) with the lowest one from 150 kHz (at the gas entrance), the O/C ratios of those two

coatings still presented a rather large variation from one another. It denotes that the energy brought by the active species (electrons, metastable species, and ions) was strong enough to influence the coating deposition and to favorize the deposition of dense carbon groups, including the formation of islands or powders. In addition, the coating analysis suggests that, despite similar energies being provided in volume when looking at the exit of the plasma zone at 35 kHz and at the entrance in the plasma zone at 150 kHz, there should still be a significant difference in the energy transfer processes.

When comparing different concentrations of the precursor, no variation of the electron temperature was observed from 250 to 350 ppm while an increase was observed at 450 ppm. Moreover, no significant influence on the argon metastable density nor on the current density was observed when increasing the proportion of the precursor. When increasing the amount of ethyl lactate molecules, the energy available per molecule considerably decreases. This means that, to activate all precursor molecules, the energy must increase, therefore explaining the rise of the electron temperature.

This was further supported by the viscous appearance of the coating when increasing the concentration of ethyl lactate, which suggests that the energy available per molecule declined such that it was no more sufficient to activate all the precursor molecules. Hence, some of the ethyl lactate ended up under its original form and deposited as liquid on the layer. This hypothesis is corroborated by the higher amount of oxygen (thus a closest O/C ratio to the ethyl lactate molecule one which is at 0.6) in the 450 ppm coating. This higher retention of the ethyl lactate molecule at low energy per molecule was also observed by Nisol et al.[21].

Changing the interelectrode gap from 1 to 2 mm did not significantly change the electron temperature and density, and the Ar metastable density. Incidentally, apart from a slight variation in the coating situated at the entrance of the carrier gas, nor the O/C ratio, the roughness or the infrared spectrum of the coating were affected by this variation, which could likely mean that the energy transfers were similar when using a 1-mm gap and a 2-mm gap. The differences observed at the coating entrance when increasing the gap likely came from turbulence in the gas flow when entering between the electrodes.

5 CONCLUSIONS

To correlate the physicochemical properties of ethyl lactate plasma-deposited polymers with the properties of argon/ethyl lactate dielectric barrier discharges, this study had two objectives. The first one aimed at evaluating the influence of various parameters on the electron temperature, argon metastable density, and electron density. To help the analysis of those results, the argon/ethyl lactate discharge was compared to an Ar-NH_3 discharge, which has been studied more extensively in literature. The second objective intended to correlate these data about the discharge with the coating deposited in such plasmas.

First of all, the low electron temperatures (from 0.3 to 0.5 eV) obtained for all discharges studied, together with a decrease of the breakdown voltage when adding ethyl lactate to a nominally pure argon discharge, suggested the dominance of the ionization of ethyl lactate by Penning reaction involving a transfer between the argon 1s states and the precursor molecule. This was corroborated by the resemblance in electron temperature and argon metastable number density between the Ar-(ethyl lactate) discharge and the Ar-ammonia discharge, which is known to be a Penning mixture.

Not all parameters studied (frequency, proportions, gap) demonstrated to have an effect on the energy brought to the discharge and on the coating deposition.

The most efficient parameter to tune the discharge behavior was found to be the frequency as it influenced all electron related behaviors (via T_e and n_e) and metastable species accumulation through a combination of electron collisions with Ar atom and memory effect. From a deposition point of view, this highly energetic plasma led to a dense and highly carbonated coating as well as to powder formation.

The proportion of the precursor had a lesser impact on the total energy transferred within the discharge, and most of it came from electron-related variations. When the energy submitted to one precursor molecule is considered, it is fair to say that the ethyl lactate proportion had a large impact. In particular, it turned out to have a massive influence on the coating density as the use of too much precursor led to the deposition of viscous-to-liquid layers.

Enlarging the gap did not demonstrate any significant variations in the plasma energetic composition as well as in the coating overall properties. Only looking at the coating at the entrance of the carrier gas in the plasma zone led to minor differences (higher carbon content and increased roughness), which were attributed to variations in the gas flow dynamics.

ACKNOWLEDGEMENTS

The authors acknowledge the Conseil franco-québécois de coopération universitaire and the National Science and Engineering Research Council (NSERC) for their financial support. We would like to thank Simon Dap from Université Paul Sabatier along with Antoine Durocher-Jean and Reetesh Gangwar from Université de Montréal for their contribution in this project.

REFERENCES

[1] Moisan P M and Pelletier D J 2012 The Plasma State: Definition and Orders of Magnitude of Principal Quantities Physics of Collisional Plasmas (Springer Netherlands) pp 1–100

[2] Hopkins M B and Graham W G 1986 Langmuir probe technique for plasma parameter measurement in a medium density discharge Rev. Sci. Instrum. 57 2210–7

[3] Lim H B and Houk R S 1990 Langmuir probe measurement of electron temperature in a supersonic jet extracted from an inductively coupled plasma Spectrochim. Acta Part B At. Spectrosc. 45 453–61

[4] Hopwood J, Guarnieri C R, Whitehair S J and Cuomo J J 1993 Langmuir probe measurements of a radio frequency induction plasma J. Vac. Sci. Technol. A 11 152–6

[5] Yanguas-Gil A, Cotrino J and González-Elipe A R 2006 Measuring the electron temperature by optical emission spectroscopy in two temperature plasmas at atmospheric pressure: A critical approach J. Appl. Phys. 99 033104

[6] Merlino R L 2007 Understanding Langmuir probe current-voltage characteristics Am. J. Phys. 75 1078–85

[7] Bogaerts A, Gijbels R and Vlcek J 1998 Collisional-radiative model for an argon glow discharge J. Appl. Phys. 84 121–36

[8] Kano K, Suzuki M and Akatsuka H 2000 Spectroscopic measurement of electron temperature and density in argon plasmas based on collisional-radiative model Plasma Sources Sci. Technol. 9 314

[9] Zhu X-M and Pu Y-K 2010 A simple collisional–radiative model for low-temperature argon discharges with pressure ranging from 1 Pa to atmospheric pressure: kinetics of Paschen 1s and 2p levels J. Phys. Appl. Phys. 43 015204

[10] Zhu X-M and Pu Y-K 2010 Optical emission spectroscopy in low-temperature plasmas containing argon and nitrogen: determination of the electron temperature and density by the line-ratio method J. Phys. Appl. Phys. 43 403001

[11] Gangwar R K, Levasseur O, Naudé N, Gherardi N, Massines F, Margot J and Stafford L 2016 Determination of the electron temperature in plane-to-plane He dielectric barrier discharges at atmospheric pressure Plasma Sources Sci. Technol. 25 1–9

[12] Bazinette R, Subileau R, Paillol J and Massines F 2014 Identification of the different diffuse dielectric barrier discharges obtained between 50kHz to 9MHz in Ar/NH3 at atmospheric pressure Plasma SOurces Sci. Technol. 23 1–9

[13] Laurent M, Koehler J, Sabbatier G, Hoesli C A, Gherardi N and Laroche G 2016 Atmospheric Pressure Plasma Polymer of Ethyl Lactate: In Vitro Degradation and Cell Viability Studies Plasma Process. Polym. 13 711–21
[14] Massines F, Gherardi N, Fornelli A and Martin S 2005 Atmospheric pressure plasma deposition of thin films by Townsend dielectric barrier discharge Surf. Coat. Technol. 200 1855–61
[15] Hegemann D, Hossain M M, Körner E and Balazs D J 2007 Macroscopic Description of Plasma Polymerization Plasma Process. Polym. 4 229–38
[16] Massines F, Sarra-Bournet C, Fanelli F, Naudé N and Gherardi N 2012 Atmospheric Pressure Low Temperature Direct Plasma Technology: Status and Challenges for Thin Film Deposition Plasma Process. Polym. 9 1041–73
[17] Golubovskii Y B, Maiorov V A, Behnke J and Behnke J F 2003 Modelling of the homogeneous barrier discharge in helium at atmospheric pressure J. Phys. Appl. Phys. 36 39
[18] Motret O, Hibert C, Pellerin S and Pouvesle J M 2000 Rotational temperature measurements in atmospheric pulsed dielectric barrier discharge - gas temperature and molecular fraction effects J. Phys. Appl. Phys. 33 1493
[19] Enache I, Caquineau H, Gherardi N, Paulmier T, Maechler L and Massines F 2007 Transport Phenomena in an Atmospheric-Pressure Townsend Discharge Fed by N2/N2O/HMDSO Mixtures Plasma Process. Polym. 4 806–14
[20] Ligot S, Renaux F, Denis L, Cossement D, Nuns N, Dubois P and Snyders R 2013 Experimental Study of the Plasma Polymerization of Ethyl Lactate Plasma Process. Polym. 10 999–1009
[21] Nisol B, Watson S, Lerouge S and Wertheimer M R 2016 Energetics of reactions in a dielectric barrier discharge with argon carrier gas: IV ethyl lactate Plasma Process. Polym. 13 965–9
[22] Desjardins E, Laurent M, Durocher-Jean A, Laroche G, Gherardi N, Naudé N and Stafford L 2017 Time-resolved study of the electron temperature and number density of argon metastable atoms in argon-based dielectric barrier discharges 23rd International Symposium on Plasma Chemistry 23rd International Symposium on Plasma Chemistry (Montréal: ISPC 23)
[23] Massines F, Gherardi N, Naudé N and Ségur P 2005 Glow and Townsend dielectric barrier discharge in various atmosphere Plasma Phys. Control. Fusion 47 577–88
[24] Pipa A V, Hoder T, Koskulics J, Schmidt M and Brandenburg R 2012 Experimental determination of dielectric barrier discharge capacitance Rev. Sci. Instrum. 83 075111
[25] Bartschat K 1999 Electron-impact excitation from the <span class Phys. Rev. A 59 2552–4
[26] Coates J 2006 Interpretation of Infrared Spectra, A Practical Approach Encyclopedia of Analytical Chemistry (John Wiley & Sons, Ltd)
[27] Kramida A, Ralchenko Y, Reader J and NIST ASD Team 2016 NIST Atomic Spectra Database Natl. Institue Stand. Technol.
[28] Chang Z-S, Yao C-W, Chen S-L and Zhang G-J 2016 Electrical and optical properties of Ar/NH3 atmospheric pressure plasma jet Phys. Plasmas 23 093503
[29] Levasseur O, Kumar Gangwar R, Profili J, Naudé N, Gherardi N and Stafford L 2017 Influence of substrate outgassing on the plasma properties during wood treatment in He dielectric barrier discharges at atmospheric pressure Plasma Process. Polym. 14 1–7
[30] Fateev A, Leipold F, Kusano Y, Stenum B, Tsakadze E and Bindslev H 2005 Plasma Chemistry in an Atmospheric Pressure Ar/NH3 Dielectric Barrier Discharge Plasma Process. Polym. 2 193–200
[31] Ligot S, Guillaume M, Gerbaux P, Thiry D, Renaux F, Cornil J, Dubois P and Snyders R 2014 Combining mass spectrometry diagnostic and density functional theory calculations for a better understanding of the plasma polymerization of ethyl lactate J. Phys. Chem. B 118 4201–11